Macromolecules

Article

pubs.acs.org/Macromolecules

Uniaxial−Biaxial Nematic Phase Transition in Combined Main-Chain/Side-Chain Liquid Crystal Polymers Using Self-Consistent Field Theory

Guang Yang, Ping Tang,* and Yuliang Yang

State Key Laboratory of Molecular Engineering of Polymers and Department of Macromolecular Science, Fudan University, Shanghai 200433, China

ABSTRACT: We investigate the isotropic−anisotropic phase transitions and the conformation of combined main-chain/side-chain liquid crystal polymers (MCSCLCPs) by numerically solving semiflexible chain self-consistent field theory (SCFT) equations with the pseudospectral method. Two kinds of interactions are involved: the global coupling between backbone segments, between the backbone and side groups, and between the side mesogens and the local coupling between the polymer backbone and its attached side groups. When the hinges are flexible, both global and local effects prefer parallel alignments of backbone and side groups, forming only prolate uniaxial nematic phase N_{PIII}. When the hinges are relatively stiff, the competition between the global interaction preferring parallel orientations of the system and the perpendicular tendency of the two components due to the comb architecture results in rich phases with various orientation modes, including uniaxial prolate phases N_{PI}, N_{PII}, and oblate phase N_O and biaxial phases N_{BI}, N_{BII}, and N_{BIII}. The new phases N_O and N_{BIII} have not yet been reported by the previous theoretical results. We conclude that the occurrence of the biaxial phases results from not only the perpendicular toplogical structures between the oriented main chain and side groups but also the bending feature of the wormlike chain backbone, another necessary condition for N_{BI} and N_{BII}.

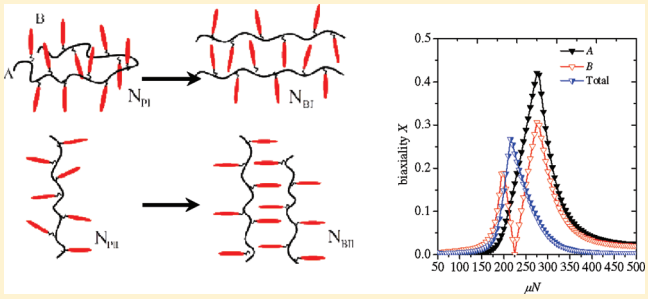

INTRODUCTION

Liquid crystal polymers (LCPs), which combine the liquid-crystalline behavior and polymeric properties, have desirable application prospects, such as optical switching and image storage, pressure and temperature sensors, shape-memory materials, protein structure studies, and so on.[1−4] LCPs have been divided into three main classes: main-chain LCPs composing of LC moiety (also called "mesogenic group") directly incorporated into backbone chain of a polymer, side-chain liquid crystal polymers (SCLCPs) in which pendant groups also playing roles as LC moiety connected to the backbone via flexible spacers,[5,6] and combined main-chain/side-chain liquid crystal polymers (MCSCLCPs), which consists of a main-chain LC backbone and side-chain LC groups.[7] In the SCLCPs, LC side groups can be linked to the backbone through either "terminal" (end-on SCLCPs) or "lateral" (side-on SCLCPs) attachment.[8] In addition, mesogen-jacked liquid crystal polymers (MJLCPs) exhibit special liquid crystal property of MCLCPs as a result of jacketing effect generated by the central rigid portion of the LC side groups laterally attached to the backbone chain without or with only quite short flexible spacers.[9] Such MJLCPs can also play the role as the semiflexible backbone in the synthesis of MCSCLCPs.[10]

During the past few decades, the complicated SCLCPs and MCSCLCPs have attracted intensive researches for academic interests on the study of the interplay of polymer chains and liquid crystal properties. Lots of experiments have devoted to investigate the influencing factors and their mutual effects on the nematic phase transitions, including the attachment (end-on or side-on SCLCPs),[11,12] the flexibility of backbone,[13,14] the length of the spacer,[15,16] molecular weight,[17,18] and mesogen graft density.[19,20] Moreover, the competition between the orientational ordering resulting from the main-chain or side-chain LC moieties and the drive to maximal entropy of the system leads to various phase structures. In order to accommodate the orientation of the LC moiety, the backbone chain coupled with the nematic ordering exhibits different conformations, including oblate ellipsoids,[11,20] prolate ellipsoids,[12,21] and biaxial phases.[10,22] Meanwhile, the orientational ordering of the LC side groups is also affected by the conformation of the backbone chain.[23] Therefore, theoretical calculation and computer simulation can help us understand the complicated phenomena of SCLCPs and MCSCLCPs.

How to describe the chain model of the system and the coupling effect on phase behavior between the main chain and side groups is the key issue in the theoretical researches on SCLCP and MCSCLCPs systems. At the earliest, Vasilenko and colleagues[24,25] developed a model by including the effect of excluded volume based on Flory type lattice theory to investigate the rodlike sections of SCLCPs. The Maier−Saupe mean-field theory which has been successfully used to understand the phase behavior of thermotropic liquid crystals was included in the SCLCPs by Brochard and co-workers[26] for

Received: December 24, 2011
Revised: March 16, 2012
Published: April 2, 2012

   dx.doi.org/10.1021/ma2027879 | *Macromolecules* 2012, 45, 3590−3603

describing the nematic interactions between liquid crystal units. They displayed the phase diagrams of the system based on Flory−Huggins theory of mixtures, whereas the backbone chain was assumed to be decoupled from the side groups. By considering the Maier−Saupe nematic interactions and the effect of chemical attachment between the backbone chain segments and the side groups, the so-called WWR model for nematic comblike polymers was proposed by Warner and co-workers.[27,28] In their work, the backbone was treated as a wormlike chain model and the rigid side groups hinged to it, as the teeth of the comb with their own mesogenic tendency. The competition between the polymers' conformational entropy and rod ordering effect resulted in three types of nematic phases depending on the volume fraction, temperature, nematic coupling, and stiffness. However, this theory treats the local stereochemical constraints on the relative orientation of backbone and its attached LC groups as a global (mean-field) interaction and gives no explanation about the influence of the spacer length on the orientational properties of the MCSCLCPs. For distinguishing these two different sources of interactions between backbone and side groups, Wessels and Mulder[6] included intrachain interactions (single-polymer effects) by hard-body repulsion between the connecting segments to mimics the stereochemical attachment. In that model, the excluded volume between the molecules had an identical formal structure for slender rods, which in some sense is unsuited to the stubby LC side groups. Recently, Wang and Wang[29] developed a freely jointed chain model by considering both the global Maier−Saupe interaction between the polymer main chain and the nematic field and the local coupling effect between the polymer backbone and its attached LC groups for investigating the thermodynamics and chain conformation of SCLCP systems. In this new model, the different behavior of side-on and end-on SCLCPs can be distinguished according to the local coupling effect supposed from experimental results, which realistically depend on the topological geometry that the point of the junction is located at the middle or at the end of the lateral group. Because correlations of global and local coupling effects on the side-on and end-on SCLCPs are different, the chain conformation of the side-on SCLCPs is always prolate and the end-on can be either oblate or prolate depending on the competitive effect of the two couplings. In general, most of the theoretical studies focused on the uniaxial nematic phases with either oblate or prolate backbone conformations,[6,29,30] while the biaxial nematic phases[10,31] and complex assembled phases in the MCSCLCPs[32] are quite limited to be theoretically studied. Considering the main-chain stiffness enhanced by the side rods and the biaxial nematic phases, the wormlike chain model[33] is suitable for describing the main chain's rigidity and the anisotropic liquid crystalline behavior of MCSCLCPs.

The self-consistent field theory (SCFT) has proved to be one of the most successful theoretical methods for investigating equilibrium phases of block copolymers[34] including comblike architectural polymers.[35] For the continuous wormlike chain model, however, solving the diffusion equation of the chain propagator $q(\mathbf{r},\mathbf{u},s)$ for describing the chain segment distribution becomes difficult due to the introduction of the extra parameter, namely a unit vector defined on a spherical surface $\mathbf{u}$ for describing the orientation of semiflexible segments. For the case of $\mathbf{r}$-independent nematic phase, the Legendre-expansion approach for solving $q(\mathbf{u},s)$, in the form of long-chain statistics, was initiated by Vroege and Odijk.[36] In the following, a spherical-harmonics expansion method coupled with real-space discretization was introduced by Cui et al.[37] to study the isotropic−nematic interface of the semiflexible polymers. Duchs and Sullivan[38] adopted the hybrid approach in ref 37 to solve the diffusion equation and study the phase behaviors of semiflexible diblock copolymers, consisting of a rigid and a flexible block. Recently, we developed a real-space method, which discretizes the orientation defined on a unit sphere with an icosahedron triangular mesh, and studied the self-assembly of semiflexible diblock copolymers both in 1D and 2D positional space implementation of SCFT.[39−41] Fredrickson[42] supposed that the pseudospectral (PS) algorithm with second-order accuracy seems be the best strategy for generating high-resolution solutions of the wormlike chain diffusion equation (Fokker−Planck equation). On the basis of the PS algorithm, Fredrickson and co-workers[43] studied the microstructures of flexible block copolymers assembled on a sphere, similar to the situation of the orientation $\mathbf{u}$ of the semiflexible segments on a unit sphere surface. In their work, a software package, SPHEREPACK 3.1,[44] was adopted for performing fast efficient transformations between the values of a 2D function $f(\mathbf{u})$ sampled on a grid on the unit sphere and its spherical harmonic coefficients. Furthermore, a SCFT model for rod−coil diblock copolymers consisting of continuous rigid rod with Maier−Saupe interaction can capture the experimental results in both bulk[45] and films[46] and is also suitable for side-chain LC block polymers.[47] Recently, a SCFT model implemented by the PS numerical approach was used to study the disorder−order transition of wormlike diblock copolymers.[48]

We develop a universal SCFT model to deal with MCSCLCPs with considering their comblike architecture and the exact connecting points of lateral groups. The MCSCLC molecules are treated as a wormlike backbone chain with its own intrinsic rigidity and nematic behavior from attached rigid rod side chains of some length to the backbone with varying flexibility hinges. The global nematic interactions favoring parallel alignment between backbone segments, between the backbone and side groups, and between the side mesogens are all described by Maier−Saupe orientational interactions. According to the experiments, if the side groups are attached to the main chain by flexible spacers (but not too long to decouple the interactions between side group and main chain), the backbone tends to parallel side groups for both end-on and side-on SCLCPs.[23,49,50] If the hinge is stiff, induced by a stiff main chain or the directly linked LC side chain, the perpendicular alignment between side groups and main chain is favorable to preserve the maximum conformational entropy.[18,20] Furthermore, the differences between side-on and end-on effects on the backbone conformation are unconspicuous once the side groups with high side-chain density dominate the phase structures, whereas the spacer length (the degree of rigidity of spacer) play important roles in the phase behaviors of SCLCPs.[15] Therefore, we use a coupling parameter μ_f proposed in ref 29 to describe the stiff extent of the attached spacer of MCSCLCPs in the form of a short-range or local interaction. $\mu_f N < 0$ prefers parallel alignments between the backbone segment and its own side group them whereas $\mu_f > 0$ represents the perpendicular attachment of the pendant. $\mu_f \leq 0$ and small values of positive μ_f indicate flexible spacers. Large value of positive μ_f indicates stiff spacers. This local coupling effect explicitly participates in the diffusion equation of the chain propagators, thus influencing the liquid crystal behavior of main and side chains. In this work, we try out the second-order pseudospectral SCFT approach with high numerical stability to

dx.doi.org/10.1021/ma2027879 | Macromolecules 2012, 45, 3590−3603

study the relatively simple nematic phase of MCSCLCPs. Not only uniaxial phases but also biaxial phases are obtained, and the effects of the stiffness of the main chain, nematic interaction, flexibility of spacer, and the component fraction on the liquid crystal behavior are investigated.

THEORETICAL FORMALISM

In this section, we briefly describe the SCFT theoretical framework for predicting the phase behavior of the MCSCLCPs. We consider incompressible side-chain polymer melts consisting of n identical polymer chains $A_{m+1}B_m$ in a volume V at the temperature T (hereafter we set $k_BT = 1$ with k_B being the Boltzmann constant). Each polymer consists of a semiflexible backbone chain denoted by A and m numbers of side rigid rods denoted by B, namely m branching points. The monomer units of semiflexible chain A and rigid rod of side chain B are characterized by statistical length a. We assume that chains A and B have the same bulk number density of the segment $\rho_0 = nN/V$, such that $ad^2 = \rho_0^{-1}$ (d is the diameter of the rod). The side chains divide the backbone chain as $m + 1$ equal parts (we called it "divided sections") with N_A segments of statistical length and each side chain B has N_B number of rod segments. N denotes the overall number of units of the side chain polymer and $N = (m + 1)N_A + mN_B$. Therefore, the volume fractions of the backbone chain A and the side groups B are given: $f_A = (m + 1)N_A/N$ and $f_B = mN_B/N$. Because the structure parameter m affects the phase diagram of the comb copolymer,[35] we fix $m = 10$ in this paper to focus on the influencing factors including the stiff extent of the main chain on the liquid crystal behaviors of MCSCLCPs. The composition of the species can be varied by changing the grafting density (the number of side chains per unit length of the backbone chain). In the results that we present, f_B is varied at the fixed N_B ($N_B = 20$), i.e., at fixed side-chain length by changing N_A. In fact, when m is fixed, the phase behavior of MCSCLCPs only depends on the radio of N_A/N_B, i.e., the volume fraction of the component f_B.

The semiflexible backbone chain A is parametrized with a continuous variable s which monotonically increases along the length of the polymer. $s = 0$ is at the beginning of backbone chain, and $s = (m + 1)N_A$ is at the other end of it. Using this parametrization, the space curves $\mathbf{r}_k(s)$ (where $k = 1, 2, ..., n$ indexes different polymers) are used to describe the different conformations of the polymer. The unit vector $\mathbf{u}_k(s)$ denotes the orientation of the kth polymer at the contour position s. Similarly, another vector $\mathbf{v}_{k,t}(s')$ ($t = 1, 2, ..., m$) denotes the orientation of the LC side group attached to the tth branching points. The nondimensional microscopic densities for the backbone chain $\hat{\phi}_A(\mathbf{r})$ and side groups $\hat{\phi}_B(\mathbf{r})$ are defined as

$$\hat{\phi}_A(\mathbf{r}) \equiv \frac{1}{\rho_0}\sum_{k=1}^{n}\int_0^{(m+1)N_A} ds\ \delta(\mathbf{r} - \mathbf{R}_k(s)) \tag{1}$$

$$\hat{\phi}_B(\mathbf{r}) \equiv \frac{1}{\rho_0}\sum_{k=1}^{n}\sum_{t=1}^{m}\int_0^{N_B} ds\ \delta(\mathbf{r} - [\mathbf{R}_k(N_At) + as\mathbf{v}_{k,t}(s)]) \tag{2}$$

Equation 2 is expressed in the form of end-on attached side groups, which can be expressed for side-on MCSCLCPs by changing the connecting points of the side groups.

In addition, the microscopic orientational order parameter for the backbone segments and side groups are defined as

$$\hat{\mathbf{S}}_A(\mathbf{r}) \equiv \frac{1}{\rho_0}\sum_{k=1}^{n}\int_0^{(m+1)N_A} ds\ \delta(\mathbf{r} - \mathbf{R}_k(s))\left(\frac{3}{2}\mathbf{u}_k\mathbf{u}_k - \frac{\mathbf{I}}{2}\right) \tag{3}$$

$$\hat{\mathbf{S}}_B(\mathbf{r}) \equiv \frac{1}{\rho_0}\sum_{k=1}^{n}\sum_{t=1}^{m}\int_0^{N_B} ds\ \delta(\mathbf{r} - [\mathbf{R}_k(N_At) + as\mathbf{v}_{k,t}(s)]) \times \left(\frac{3}{2}\mathbf{v}_{k,t}(s)\mathbf{v}_{k,t}(s) - \frac{\mathbf{I}}{2}\right) \tag{4}$$

where $\mathbf{I}$ is a 3×3 unit matrix. The incompressibility constraint is provided by enforcing that

$$\hat{\phi}_A(\mathbf{r}) + \hat{\phi}_B(\mathbf{r}) = 1 \tag{5}$$

Energetic interactions in the above model consist of the following four components:

$$H_1 = \frac{\xi}{2}\sum_{k=1}^{n}\int_0^{(m+1)N_A} ds\left|\frac{d\mathbf{u}_k(s)}{ds}\right|^2 \tag{6}$$

describing the total bending energy for the semiflexible components of the backbone chain with side rods attached, where ξ is the persistent length

$$H_2 = -\frac{\chi}{4}\int d\mathbf{r}\,(\hat{\phi}_A(\mathbf{r}) - \hat{\phi}_B(\mathbf{r}))^2 \tag{7}$$

describing the isotropic repulsion between unlike segments A and B, where χ is the Flory–Huggins interaction parameter between these segments which favors their phase separation

$$H_3 = -\frac{\mu_{AA}}{2}\int d\mathbf{r}\,\hat{\mathbf{S}}_A(\mathbf{r}):\hat{\mathbf{S}}_A(\mathbf{r}) - \frac{\mu_{BB}}{2}\int d\mathbf{r}\,\hat{\mathbf{S}}_B(\mathbf{r}):\hat{\mathbf{S}}_B(\mathbf{r}) - \mu_{AB}\int d\mathbf{r}\,\hat{\mathbf{S}}_A(\mathbf{r}):\hat{\mathbf{S}}_B(\mathbf{r}) \tag{8}$$

describing the Maier–Saupe interaction energy, where $\mu_{\kappa,\kappa'}$ ($\kappa, \kappa' = A, B$) represents the strength of anisotropically orientational interaction favoring the parallel alignment of orientational units, and

$$H_4 = \mu_f\sum_{k=1}^{n}\sum_{t=1}^{m}(\mathbf{u}_k(N_At)\cdot\mathbf{v}_{k,t}(0))^2 \tag{9}$$

indicating the local effect of flexibility of the spacer on the orientational alignment between the main chain and the side segments. Equation 9 representing the local coupling effect, was originally proposed in ref 29 where $\mu_f < 0$ represents side-on and $\mu_f > 0$ represents end-on SCLCPs, which are assumed to be determined by some experimental results. In our work, $\mu_f \leq 0$, indicating flexible spacers between the backbone segment and its own side group, and $\mu_f > 0$, preferring perpendicular attachment due to a stiff hinge.

Therefore, the partition function of the system is

$$Z \propto \int D\mathbf{R}_k(s)d\mathbf{u}_k(s)\delta\left[\mathbf{u}_k(s) - \frac{d}{ds}\mathbf{R}_k(s)\right]\delta[|\mathbf{u}_k(s)| - 1] \times \sum_{t=1}^{m}d\mathbf{v}_{k,t}(s')\exp[-\rho_0(H_1 + H_2 + H_3 + H_4)] \times \delta(\hat{\phi}_A(\mathbf{r}) + \hat{\phi}_B(\mathbf{r}) - 1) \tag{10}$$

dx.doi.org/10.1021/ma2027879 | Macromolecules 2012, 45, 3590–3603

By employing standard field-theoretical techniques, the quadratic interactions in the Hamiltonian can be decoupled by introducing fluctuating chemical potential fields with respect to the density and orientational order parameters.[51] In a nondimensional representation, all length scales of the system are denoted by the contour length $L \equiv aN$, and the continuous variable s and persistent length ξ are normalized by the overall molecular weight N. The partition function can be rewritten as a functional integral

$$Z \propto \prod_{P=A,B} \int D\phi_P D\omega_P \int D\eta D\mathbf{S}_P D\mathbf{M}_P \exp(-\rho_0 F) \tag{11}$$

The free energy per polymer chain is

$$\begin{aligned}\frac{\rho_0 F}{n} = \frac{1}{V}\int d\mathbf{r}\,[\chi N\phi_A(\mathbf{r})\phi_B(\mathbf{r}) - \sum_{P=A,B}\omega_P(\mathbf{r})\phi_P(\mathbf{r}) \\ + \eta(\mathbf{r})\Big(\sum_{P=A,B}\phi_P(\mathbf{r}) - 1\Big) - \frac{\mu_{AA}N}{2}\mathbf{S}_A(\mathbf{r}) \\ : \mathbf{S}_A(\mathbf{r}) - \frac{\mu_{BB}N}{2}\mathbf{S}_B(\mathbf{r}) : \mathbf{S}_B(\mathbf{r}) - \mu_{AB}N\mathbf{S}_A(\mathbf{r}) \\ : \mathbf{S}_B(\mathbf{r}) + \mathbf{M}_A(\mathbf{r}) : \mathbf{S}_A(\mathbf{r}) + \mathbf{M}_B(\mathbf{r}) : \mathbf{S}_B(\mathbf{r})] - \ln Q\end{aligned} \tag{12}$$

In the above equations, $\omega_P(\mathbf{r})$ is a purely imaginary conjugate field to the densities with species $P = (A,B)$, and $\eta(\mathbf{r})$ ensures the incompressibility of the system. $\mathbf{M}_P(\mathbf{r})$ is purely imaginary conjugate tensorial orientation field to the orientational parameter $\hat{\mathbf{S}}_P$. Q represents the single chain partition function of a MCSCLC polymer under the external fields $\omega_P(\mathbf{r})$, $\eta(\mathbf{r})$, and $\mathbf{M}_p(\mathbf{r})$, which is given by

$$\begin{aligned}Q \equiv \int D\mathbf{R}\,d\mathbf{u}\,d\mathbf{v}\,\delta\Big[\mathbf{u}(s) - \frac{d}{L\,ds}\mathbf{R}(s)\Big]\delta[|\mathbf{u}(s)| - 1] \\ \times \exp\Big\{-\frac{\xi}{2}\int_0^{f_A} ds\,\Big|\frac{d\mathbf{u}(s)}{ds}\Big|^2\Big\} \\ \times \exp\Big\{-\int_0^{f_A} ds\Big[\omega_A(\mathbf{R}(s)) - \mathbf{M}_A(\mathbf{R}(s)) : \Big(\frac{3}{2}\mathbf{uu} - \frac{\mathbf{I}}{2}\Big)\Big]\Big\} \\ \times \exp\{-\sum_{t=1}^{m}\int_0^{f_B/m} ds'[\omega_B(\mathbf{R}(tN_A/N) + Ls'\mathbf{v}_t(s')) \\ - \mathbf{M}_B(\mathbf{R}(tN_A/N) + Ls'\mathbf{v}_t(s')) : \Big(\frac{3}{2}\mathbf{v}_t\mathbf{v}_t - \frac{\mathbf{I}}{2}\Big)]\} \\ \times \exp[-\mu_f N\sum_{t=1}^{m}(\mathbf{u}(tN_A/N)\cdot\mathbf{v}_t(0))^2]\end{aligned} \tag{13}$$

According to the mean-field approximation, the complete SCFT equations for SCLCPs are obtained by minimizing the free energy functional eq 12 with respect to $\phi_P(\mathbf{r})$, $\omega_P(\mathbf{r})$, $\eta(\mathbf{r})$, $S_P(\mathbf{r})$, and $M_P(\mathbf{r})$. To reduce computational loads, we restrict the present study to only consider the nematic phases of the MCSCLCPs; thus, the density fields and orientation fields are homogeneous in the positional space; i.e., $\phi_A(\mathbf{r})$, $\phi_B(\mathbf{r})$, $\mathbf{S}_A(\mathbf{r})$, and $\mathbf{S}_B(\mathbf{r})$ reduce to f_A, f_B, $\mathbf{S}_A$, and $\mathbf{S}_B$, respectively. We should note that the side-on and end-on MCSCLCPs determined by the positional related fields in eq 13 could not be distinguished due to ignorance of heterogeneous phase in positional space. We further assume that each of the graft side groups are in the same conditions of the orientational fields, thus replacing $\mathbf{v}_t$ with $\mathbf{v}$. According to the above treatments, the free energy reduces as follows:

$$\begin{aligned}F = -\frac{\mu_{AA}N}{2}\mathbf{S}_A : \mathbf{S}_A - \frac{\mu_{BB}N}{2}\mathbf{S}_B : \mathbf{S}_B - \mu_{AB}N\mathbf{S}_A \\ : \mathbf{S}_B + \mathbf{M}_A : \mathbf{S}_A + \mathbf{M}_B : \mathbf{S}_B - \ln Q\end{aligned} \tag{14}$$

Minimizing the functional F, the SCFT equations are expressed as follows:

$$\mathbf{M}_A = \mu_{AA}N\mathbf{S}_A + \mu_{AB}N\mathbf{S}_B \tag{15}$$

$$\mathbf{M}_B = \mu_{BB}N\mathbf{S}_B + \mu_{AB}N\mathbf{S}_A \tag{16}$$

$$\begin{aligned}\mathbf{S}_A = \frac{1}{Q\int d\mathbf{u}}\sum_{t=1}^{m+1}\int_0^{N_A/N} ds\int d\mathbf{u}\,q(\mathbf{u}, s, t) \\ \times q(\mathbf{u}, N_A/N - s, m + 1 - t)\Big(\frac{3}{2}\mathbf{uu} - \frac{\mathbf{I}}{2}\Big)\end{aligned} \tag{17}$$

$$\begin{aligned}S_B = \frac{N_B}{NQ\int d\mathbf{u}\int d\mathbf{v}}\sum_{t=1}^{m}\int d\mathbf{u}\,d\mathbf{v}\,q(\mathbf{u}, N_A, t) \\ \times q(\mathbf{u}, N_A, m - t)\exp[-\mu_f N(\mathbf{u}\cdot\mathbf{v})^2] \\ \times \exp\Big[-\frac{N_B}{N}\Gamma_B(\mathbf{v})\Big]\Big(\frac{3}{2}\mathbf{vv} - \frac{\mathbf{I}}{2}\Big)\end{aligned} \tag{18}$$

where

$$Q = \frac{1}{\int d\mathbf{u}}\int d\mathbf{u}\,q(\mathbf{u}, N_A/N, m + 1) \tag{19}$$

The chain propagator of $m + 1$ sections of main chain $q(\mathbf{u},s,t)$ corresponds to the probability of finding a partial backbone chain of length $s \in [0, N_A/N]$ that starts from the end of each divided sections of A ($s = 0$) with the orientation $\mathbf{u}$, which satisfies the modified diffusion equation:

$$\begin{aligned}\frac{\partial q(\mathbf{u}, s, t)}{\partial s} = -\Gamma_A(\mathbf{u})q(\mathbf{u}, s, t) + \frac{1}{2\xi}\nabla_u^2 q(\mathbf{u}, s, t) \\ t = 1, 2, ..., m + 1\end{aligned} \tag{20}$$

The $\mathbf{r}$-independent diffusion equation in the external field is similar to that used by Chen[52] for studying the nematic ordering of semiflexible polymers. The initial conditions for the diffusion equation are

$$\begin{aligned}q(\mathbf{u}, 0, 1) = 1 \\ q(\mathbf{u}, 0, t + 1) = \Big\{q(\mathbf{u}, N_A/N, t)\int d\mathbf{v}\exp\Big[-\frac{N_B}{N}\Gamma_B(\mathbf{v})\Big] \\ \times \exp[-\mu_f N(\mathbf{u}\cdot\mathbf{v})^2]\Big\}/\int d\mathbf{v}\end{aligned} \tag{21}$$

where

$$\Gamma_A(\mathbf{u}) = -\mathbf{M}_A : \Big(\frac{3}{2}\mathbf{uu} - \frac{\mathbf{I}}{2}\Big) \tag{22}$$

$$\Gamma_B(\mathbf{v}) = -\mathbf{M}_B : \Big(\frac{3}{2}\mathbf{vv} - \frac{\mathbf{I}}{2}\Big) \tag{23}$$

dx.doi.org/10.1021/ma2027879 | Macromolecules 2012, 45, 3590−3603

Equations 15−18 form a closed set of self-consistent equations, which can be numerically implemented by combinatorial screening algorithm for Gaussian chain SCFT equations proposed by Drolet and Fredrickson.[34] In our work, the diffusion equation (20) is solved to obtain $q(\mathbf{u},s,t)$ with the pseudospectral (PS) operator splitting algorithm:[42,43]

$$q(\mathbf{u}, s + \Delta s, t) = \exp(-\Gamma(\mathbf{u})\Delta s/2) \exp\left(\frac{\Delta s}{2\xi}\nabla_{\mathbf{u}}^2\right) \times \exp(-\Gamma(\mathbf{u})\Delta s/2) q(\mathbf{u}, s, t) \quad (24)$$

The unit vector $\mathbf{u}$ is oriented in the three-dimensional plane, i.e., $\mathbf{u} = \mathbf{e}_x \sin\theta\cos\varphi + \mathbf{e}_y \sin\theta\sin\varphi + \mathbf{e}_z \cos\theta$. The software package "Spherepack 3.2"[44] enables us to evaluate the Laplacian of a function $f(\mathbf{u})$, i.e., $f(\theta,\phi)$, by implementing an efficient transforming between gird points on the sphere and its spherical harmonic coefficients. In this work, we perform the angular discretization through a 17-point evenly distributed points for θ and a 32-point evenly distributed points for ϕ. The discretization of contour variable s is chosen to be Δs = 0.002. In order to obtain relatively stable phases, we start the calculation referring to the Drolet Fredrickson combinatorial search[34] with both random initial orientation fields and completely aligned states including uniaxial and biaxial initial fields by ranging θ and ϕ from 0 to $\pi/2$, respectively. The final stable phase structure is thus determined as the one having the lowest free energy. Furthermore, the pseudodynamical evolutions are carried out to a convergence of 10^{-7} in free energy and a convergence of 10^{-4} in fields values. By contrast, we also perform the real-space solution of the diffusion equation (20) as developed in our previous work,[39] in which $\mathbf{u}$ on the spherical surface is discretized into icosahedron triangular mesh with M number of vertexes. Our tests show that the discrete points of s are at least twice of those in the above-mentioned PS method to ensure the numerical stability with the convergence of 10^{-5} in the free energy. Moreover, the PS method has faster convergences of the free energy and fields than the real-space method.

RESULTS AND DISCUSSION

According to our model, there are six factors influencing the nematic phase behaviors of MCSCLCPs including the main chain stiffness ξ, the orientational interactions between main chains $\mu_{AA}N$ and the side chain groups $\mu_{BB}N$, the volume fraction f_B, the global coupling effect $\mu_{AB}N$ preferring the anisotropic interactions between components A and B, and the local coupling effect μ_fN representing the spacers' flexibility. In the simulations of our explored parameter space, we obtain not only the uniaxial nematic phase but also complex biaxial nematic phase by varying the hinges flexibility μ_fN. It is common to construct MCSCLCPs with different hinge flexibility by altering the chemical composition of a spacer unit. When $\mu_fN \le 0$, MCSCLCPs have flexible spacers and favor parallel ordering between main chain and side groups. In this case, both the global interactions and local coupling play synergistic roles in the orientation of the system, favoring prolate conformation, as discussed in ref 29. Thus, we first focus on the influence of global interactions $\mu_{AB}N$ at different values of ξ and f_B in the absence of μ_fN, i.e., $\mu_fN = 0$. In fact, $\mu_fN = 0$ means that the side groups are decoupled from the backbone due to a very long or flexible spacer. We also consider the system conformation with different degree of main chain's rigidity including relatively flexible case ($\xi \le 0.1$) for comparison with the results reported in ref 29. When the side groups perpendicular attached to main-chain segment, i.e., $\mu_fN > 0$, more complex uniaxial and biaxial phase transitions occur. With the increase of the hinges stiffness, the phase behaviors become more complicated. In the case of the semiflexible main chain ($\xi = 1$), we investigate the phase transitions depending on the relationships between μ_fN, $\mu_{AA}N$, $\mu_{BB}N$, and $\mu_{AB}N$. Furthermore, the phase diagram in the μN−f_B plane in the case of $\mu_fN = 0.5\ \mu N$ is shown for $\xi = 1$. In our simulations, if all the global interactions $\mu_{AA}N$, $\mu_{BB}N$, and $\mu_{AB}N$ are considered to exist in the system, we assume $\mu_{AA} = \mu_{BB} = \mu_{AB} = \mu$ to simplify the influences of the chemical structure difference between A and A, B and B, and A and B.

A. Defining Various Nematic Phases. Molecular uniaxiality and biaxiality are two main characteristics for the ordering of nematic phase.[5] The uniaxial phase has the main directions of the molecules, which tend to be symmetrically parallel to the same common axis, while the biaxial phase can be expected with building blocks shaped in the form of long rectangles. For MCSCLCPs, however, even with main and side chains being geometrically uniaxial, biaxial phases may emerge because of the branch geometry,[16,22,31] quite different from the biaxial phase observed experimentally[53,54] in low molecular weight liquid crystals. In the self-consistent field theory of MCSCLCP system, the nematic phase is characterized by the Maier−Saupe orientational order parameter of the constituent species $\mathbf{S}_P$ (P = A, B), which is a traceless symmetric second-rank tensor. We normalize the orientational order parameter by volume fraction of A and B, respectively, i.e., $\mathbf{T}_P = \mathbf{S}_P/f_P$. After diagonalization of this orientational tensor, it becomes $\mathbf{T}_P = [\lambda_{x,P}\ \lambda_{y,P}\ \lambda_{z,P}]^{\mathrm{T}}\ \mathbf{I}$ with $\lambda_{x,P} + \lambda_{y,P} + \lambda_{z,P} = 0$. The average order parameters, i.e., eigenvalues elements $\lambda_{x,P}$, $\lambda_{y,P}$, and $\lambda_{z,P}$, determine the degree of orientations of main chain and side groups in x-, y-, and z-directions. We assume that $|\lambda_z|$ is always larger than $|\lambda_x|$, and $|\lambda_y|$; i.e., the principal axis is chosen as the z-directional orientation.

The normal convention of the uniaxial nematic phase ordered in the z-direction (main director) is that $\lambda_x = \lambda_y = -0.5\lambda_z$, and only one scalar order parameter λ_z is needed. $\lambda_z \in (0,1]$ represents prolate (rodlike) conformation while $\lambda_z \in [-0.5,0)$ represents oblate (disklike) conformation. Biaxial nematic phases exhibit additional orientational order of the system along a second macroscopic direction, the "short" axis, perpendicular to the primary nematic director. Therefore, after extracting the largest element $|\lambda_z|$ of the order parameter matrix, the biaxiality parameter is determined by the difference between the other two elements $X = |\lambda_x - \lambda_y|$. Therefore, $X = 0$ for uniaxial nematic phase while $\lambda_x \ne \lambda_y$ for biaxial nematic phase, in which two independent order parameters, λ_z and X, are required[31]

$$\lambda_x = -\frac{1}{2}\lambda_z + \frac{1}{2}X,\ \lambda_y = -\frac{1}{2}\lambda_z - \frac{1}{2}X \quad (0 \le X \le 0.5) \quad (25)$$

Because of the individual orientations of components A and B, they can create synergies for the entire system orientation and also can cancel out the effect of each other. With the assumed condition $\mu_{AA} = \mu_{BB} = \mu_{AB} = \mu$, there are only one united tensorial orientation field influencing the order parameters of the system, i.e., $\mathbf{M}_A = \mathbf{M}_B$. Therefore, the chain conformation of the overall system, λ_T, can be evolved from the order parameter of overall system, $\mathbf{T}_T = (\mathbf{S}_A + \mathbf{S}_B)/(f_A + f_B)$. The biaxiality of

dx.doi.org/10.1021/ma2027879 | Macromolecules 2012, 45, 3590−3603

the overall system is represents as X_T. For clarity, we use the symbols P_A, O_A, and B_A to note prolate, oblate, and biaxial phases of the main chain and P_B, O_B, and B_B for side groups, respectively. Previous theoretical work reported $N_{PI}(O_AP_B)$, $N_{PII}(P_AO_B)$, $N_{PIII}(P_AP_B)$[27,29] and biaxial phase $N_{BI}(B_AP_B)$ and $N_{BII}(P_AB_B)$,[31] with the schematics shown in Figure 1. Bladon et al.[31]

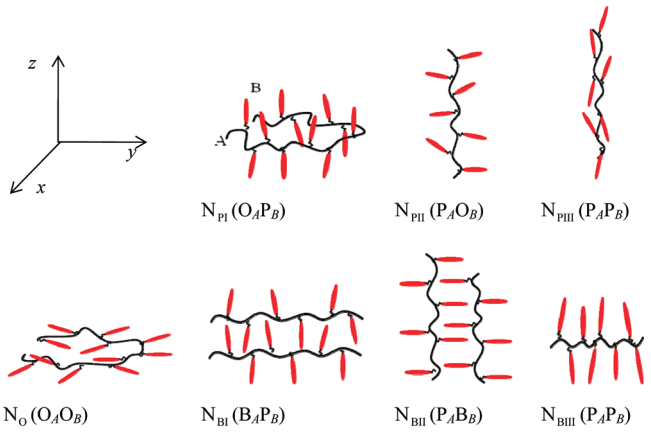

Figure 1. Schematic illustration of the nematic phase for end-on MCSCLCPs. P_A, O_A, and B_A indicate the prolate ellipsoidal order, oblate ellipsoidal order, and biaxial flat plane of the main chain A and P_B, O_B, and B_B for side groups B, respectively. $N_{PI}(O_AP_B)$, $N_{PII}(P_AO_B)$, and $N_{PIII}(P_AP_B)$ are uniaxial phases with prolate ellipsoid shapes; $N_O(O_AO_B)$ is uniaxial phase with oblate ellipsoid shape; $N_{BI}(B_AP_B)$, $N_{BII}(P_AB_B)$, and $N_{BIII}(P_AP_B)$ are biaxial phases. $N_{BI}(B_AP_B)$ and $N_{BII}(P_AB_B)$ signify that biaxialities are mainly contributed from A and B, respectively. The new phases N_O and N_{BIII} have not yet been reported in previous theoretical work.

suggested that N_{BI} and N_{BII} are evolved from N_{PI} and N_{PII}, respectively. The biaxial phase actually adopts a flattened prolate ellipsoidal shape with one of the components parallel to the z-direction and another ordered almost uniaxially along the x- or y-direction. If the largest value of uniaxial order parameter is given by the side-chain (main-chain) component, the phase is called N_{BI} (N_{BII}). We should note that the two phases are physically identical and simply related by a spatial rotation because the system is a flattened prolate ellipsoidal shape in the coordinate system.[31] In fact, for the biaxial phases N_{BI} and N_{BII} in our study, A and B each almost has a separate major axis of symmetry. In order to simplify the phase diagram, we will no longer distinguish them from N_{BI} or N_{BII}. In particular, we find two new phases shown in Figure 1. One is $N_O(O_AO_B)$ phase with both of the components displaying oblate shapes and orienting parallelly between each other, which is typically found when the orientations of A and B are comparable. Another new phase is a biaxial phase denoted as $N_{BIII}(P_AP_B)$ where both A and B present prolate shapes and perpendicularly orient along their individual primary directions. This phase occurs at quite large volume fractions of B and perpendicular oriented hinge units between the relativley stiff backbone and side groups.

B. Prolate Uniaxial Nematic Phase in the Case of $\mu_f N = 0$. For $\mu_f N = 0$, the tendency of mutual orthogonal orientation between main chain and side groups disappears, corresponding to the case of quite flexible hinges. The N_{PIII} phase, prolate ellipsoidal shape formed both by main chain A and side groups B, is obtained, because all the individual orientation interactions $\mu_{AA}N$ and $\mu_{BB}N$ and the global coupling $\mu_{AB}N$ all favor parallel orientations of LC side group and main chain segment. It was confirmed by the experiments that the natural tendency of the backbone chain was to adopt a prolate shape in the nematic phase when the hinges were flexible; i.e., the spacers connecting backbone and side groups were long enough.[49,55] We take the parameters of $\mu_f N = 0$, $\xi = 1$, $\mu_{AA} = \mu_{BB} = \mu_{AB} = \mu$ and $f_B = 0.476$ ($N_A/N_B = 1$) as an example to describe the I–N_{PIII} phase transition, as shown in Figure 2. The average order parameters

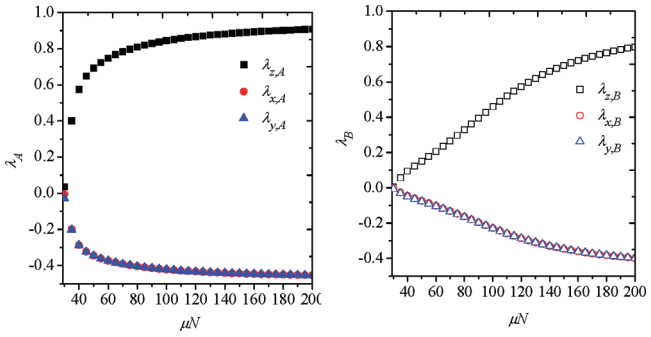

Figure 2. Orientational order parameters λ for MCSCLCPs with $f_B = 0.476$ ($N_A/N_B = 1$) and $\xi = 1$ as a function of orientational interaction μN in the case of $\mu_f N = 0$ and $\mu_{AA}N = \mu_{BB}N = \mu_{AB}N = \mu N$.

λ_A of the main chain increase rapidly with the μN increasing to 35, with $\lambda_{z,A} > 0$ and $\lambda_{x,A} = \lambda_{y,A}$ representing a uniaxial prolate spheroid of main chain A. At the same time, the side chains B begin to order in parallel with A, presenting prolate shape as well as A forming the N_{PIII} phase. Furthermore, $\lambda_{z,B}$ increases linearly when μN is increased from 35 to 130, whereas $\lambda_{z,A}$ increases rapidly to a high value ($\lambda_{z,A} = 0.8$) at $\mu N = 85$ and the value of $\lambda_{z,B}$ is always less than that of A at the same μN. This phenomenon indicates that the main chain A with some stiffness in this case dominates the ordering of nematic phases of MCSCLCPs.

I–N_{PIII} Phase Transition without Global Coupling ($\mu_{AB}N = 0$). In order to explore the interaction effects between main chain A and side groups B, we separate them by ignoring both global and local coupling effects between them, i.e., $\mu_{AB}N = 0$ and $\mu_f N = 0$. In the work of ref 29, the LC behavior of flexible backbone chains is induced by the orientation of rigid side groups; thus, the backbone chain remains isotropic when neglecting both global and local coupling effects. However, in our model, the main chain can also have LC behavior because of its instinct rigidity even without the global and local coupling effects. The transitions between isotropic phase and prolate nematic phase with different backbone's rigidities ξ are shown in Figure 3. In this case, the orientations of A and B have no relationship between each other. The ordering of A depends only on ξ, whereas that of B depends only on the structure parameter m. As long as ξ and m are fixed, the degrees of the ordering of main chain and side groups are relative to their individual self-orientation interactions, $\mu_{AA}N$ and $\mu_{BB}N$. The behavior of side groups B dominates in the right of the phase diagram because the strength of side-chain interaction governed by their volume fraction f_B is over the main chain. However, for the main chain, the effect of orientation not only depends on its volume fraction but also has relationship with ξ, thus displaying higher I–N_{PIII} for the case of low rigidity ($\xi = 0.1$) than that of $\xi = 1$. It should be noticed that the two components A and B still tend to be parallel to each other. According to mean-field Maier–Saupe orientational interactions adopted in our model, the parallel alignment of the orientation between backbone and

dx.doi.org/10.1021/ma2027879 | Macromolecules 2012, 45, 3590–3603

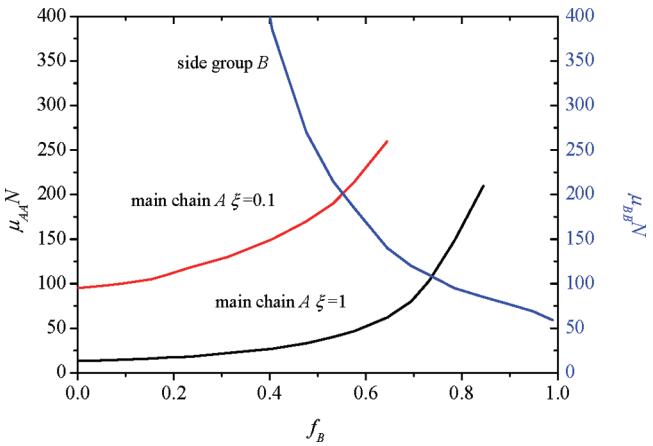

Figure 3. Phase transition lines from isotropic to prolate-shaped anisotropic phase for main chain *A* and side groups *B* plotted in the $\mu_{AA}N$–f_B and $\mu_{BB}N$–f_B planes without the global ($\mu_{AB}N = 0$) and local ($\mu_f N = 0$) coupling effects. The transition lines for *A* only depend on the stiffness ξ, and thus $\xi = 1$ and $\xi = 0.1$ are considered for comparison.

side groups remains to exist even in the case of $\mu_f N = 0$ and $\mu_{AB}N = 0$.

I–N_{PIII} Phase Transition in the Presence of Global Coupling ($\mu_{AB}N \neq 0$). The global coupling effect $\mu_{AB}N$ strengthens the parallel alignments of main chain *A* and side groups *B*. In this work, we combine them by using a uniform parameter μN ($\mu_{AB}N = \mu_{AA}N = \mu_{AB}N = \mu N$), and the I–$N_{PIII}$ phase transition is obtained when $\mu_f N = 0$. Figures 4a and 4b indicate the phase diagram plotted in the μN–f_B plane with relatively stiff main chain *A* ($\xi = 1$) and relatively flexible *A* ($\xi = 0.1$). The solid lines separate the uniaxial nematic phase N_{PIII} from isotropic phase I, and the dashed curves are chosen at an arbitrary value of $\lambda_{z,P} = 0.2$ for *A* and *B*, respectively. In Figure 4a, the main chain *A* with $f_B = 0$ begins to order at $\mu N = 13$ for $\xi = 1$. With the increase of f_B, the critical values of μN at the phase transition, noted as $(\mu N)_C$, enlarge with positive deviation from linear increase relationship. In the region of $0.5 < f_B < 0.89$, the change trend of $(\mu N)_C$ is negative deviation from linear increase. The value of $(\mu N)_C$ decreases when $f_B > 0.89$ and approaches $(\mu N)_C = 70$ with f_B being close to 1. One of the dashed curves representing *A* nearly coincides with the phase transiton line, but the other dashed curve representing *B* has relatively large disparity at small f_B. In contrast to the stiff main chain, the phase transition of relatively flexible main chain ($\xi = 0.1$) is shown in Figure 4b, which needs larger values of μN (lower temperature) compared with the case of $\xi = 1$. It is consistent with the experimental result of MCSCLCPs that enhancing the stiffness of the backbone gives rise to the nematic order of the system.[14] Moreover, the value of $(\mu N)_C$ increases initially before reaching the largest value at $f_B = 0.35$ when f_B is increased from 0.05 to 0.95. The highly ordered *A* and *B* (separated by dashed lines) appears simultaneously after $f_B = 0.35$.

The global interaction $\mu_{AB}N$ as well as different stiffness ξ of the main chain has significant effects on the I–N_{PIII} phase transition. The competition between the tendency to maximize the conformation entropy of main chain with different stiffness and the orientational order induced by the LC character of the system leads to the phase performances of MCSCLCPs. Thus, in Figure 4a, the LC behavior of the main chain *A* plays a great role for relative stiff backbone ($\xi = 1$) and the dashed line ($\lambda_{z,A} = 0.2$) presenting *A* nearly coincides with phase transition line. The addition of small volume fraction of *B* ($f_B < 0.5$) requires lower temperature to be ordered, thus leading to slightly higher of the transition line of the system than that of *A* in Figure 3. However, for relatively flexible backbone ($\xi = 0.1$), the phase transition occurs at large values of μN because the maximal conformation entropy of flexible chain controls over the ordering interactions of main-chain segments. This phenomenon is in agreement with the experimental result that increasing backbone's flexibility appeared to decrease the clearing temperature (larger μN was required to produce liquid crystal behavior) for the MCSCLCPs.[13] In this case, the side groups dominate the orientation of the system and the main chain and the overall system both display stronger orientations as the volume fraction of the side groups f_B is largely increased. The apparent persistence length seems to be increased due to the global interactions of the systems rather than the instinct property of MCSCLCPs, which is coincident with the experiment result.[18,19]

It is noted that our model also works for investigating the conformation of SCLCPs with quite flexible main chain.

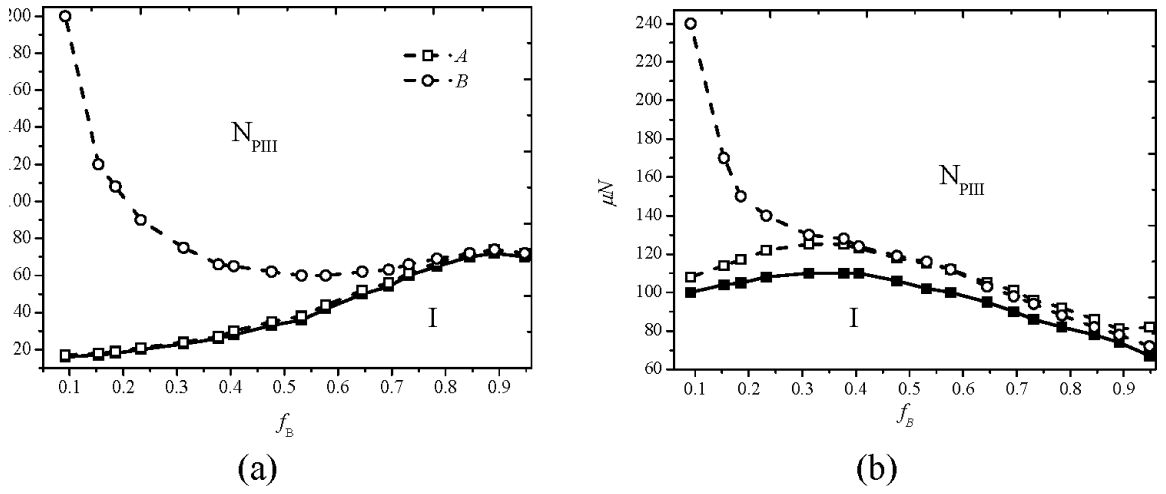

Figure 4. Phase diagram plotted in the μN–f_B plane for the MCSCLCPs with varying main-chain stiffness when $\mu_f N = 0$. (a) $\xi = 1.0$; (b) $\xi = 0.1$.

dx.doi.org/10.1021/ma2027879 | *Macromolecules* 2012, 45, 3590–3603

The mean-squared end-to-end distance vector for the wormlike chain satisfies the Kratky−Porod expression:[33]

$$\langle R^2\rangle = 2\xi L\left\{1 - \frac{\xi}{L}[1 - \exp(-L/\xi)]\right\} \quad (26)$$

In the flexible limit, $L/\xi \gg 1$, we obtain $R \approx (2\xi L)^{1/2}$, which is consistent with the ideal Gaussian chain scaling formula $R = bN^{1/2}$ if we define the contour length $L = Nb$ and $b = 2\xi$. In the rigid rod limit, i.e., $L/\xi \ll 1$, $R = L$. Therefore, the wormlike chain model allows perfect crossover from flexible chain to rigid rod chains. In our work, we set $\xi \leq 0.1$ for the relatively flexible polymer backbone, and in this case, the statistical behavior of the wormlike chain approaches that of the freely jointed chains. Therefore, conformation anisotropic radios $R_{\|}/R_{\perp}$ can be approximately calculated based on freely jointed chain model. We compare the conformation anisotropic radios $R_{\|}/R_{\perp}$ of the relatively flexible polymer backbone in uniaxial phases N_{PIII} with the results reported in ref 29. $\langle R_{\|}^2\rangle$ is the mean-square end-to-end distance vector in the direction parallel to the nematic axis (denoted along the z-direction), which is given by

$$\langle R_{\|}^2\rangle = \langle R_g^2\rangle\left(\frac{1}{3} + \frac{2}{3}\lambda_z\right) \quad (27)$$

where $\langle R_g^2\rangle$ is the mean-square radius of gyration for the wormlike chain with some given ξ values in the isotropic phase. $\langle R_{\perp}^2\rangle$ is the mean-square end-to-end distance vector in the perpendicular direction, which is given by

$$\langle R_{\perp}^2\rangle = \langle R_g^2\rangle\left(\frac{1}{3} - \frac{1}{3}\lambda_z\right) \quad (28)$$

Figure 5 shows the changes of the ratio $R_{\|}/R_{\perp}$ with respect to $\mu N - \mu N^*$ at different values of ξ. μN^* is the corresponding critical value of the orientational interaction at the phase transition. Similar to the analysis mentioned above, μN^* increases when the main chain becomes more flexible from $\xi = 0.1$ to $\xi = 0.05$ to $\xi = 0.01$, and the values of μN^* are 115, 165, and 260, respectively. For the most flexible main chain ($\xi = 0.01$), the degree of anisotropy, i.e., the ratio $R_{\|}/R_{\perp}$, increases slowly with increasing μN or decreasing the temperature. The coupling effect favoring parallel ordering between main chain and side groups is in agreement with that reported in ref 29.

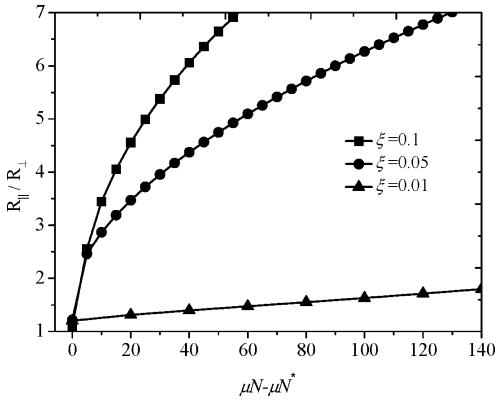

Figure 5. Main-chain conformation anisotropic ratio $R_{\|}/R_{\perp}$ for relatively flexible main chain ($\xi = 0.1$, $\xi = 0.05$, and $\xi = 0.01$) with $f_B = 0.476(N_A/N_B = 1)$ as a function of Maier−Saupe interaction $\mu N - \mu N^*$ under $\mu_f N = 0$. μN^* is the corresponding critical value at the phase transition.

However, compared to their results, the anisotropy radio of such a flexible main chain is smaller even with a large value of μN in our work. This is reasonable because the maximal conformation entropy of flexible chain dominates over the ordering between the main chain and side groups of the SCLCPs' phase behavior. Furthermore, we notice that the main chain's flexibility has strong influence on the conformation of the backbone. The relatively stiff main chains with larger value of ξ likely emerge anisotropic performances and can order strongly with large value of the anisotropy radio. The more stiffness the main chain possesses, the stronger tendency of the parallel alignment of the main chain segments.

C. Uniaxial to Biaxial Phase Transition in the Case of $\mu_f N > 0$. When the side groups are connected to the main chain via a short spacer or only a single covalent bond, we regard the hinges as being stiff. In this case, a perpendicular ordering alignment structure between backbone chain and side groups tends to form, denoted as $\mu_f N > 0$. There are two kinds of competitions in the MCSCLCPs. On one hand, the stretching energy of main chain with some bending modulus ξ must balance its conformation entropies, and the conformation will disturb the parallel alignment of side groups in some extent. On the other hand, the competitions between the global Maier−Saupe interaction preferring parallel ordering of main chain and side groups and the perpendicular tendency of the two components enhance the complexity of the MCSCLCPs phase behavior. Therefore, some complex phases are found, including uniaxial nematic phase N_{PI}, N_{PII}, and N_O and biaxial phase N_{BI}, N_{BII}, and N_{BIII}, which have been briefly introduced in section A. In this section, we first fix the volume fraction $f_B = 0.476(N_A/N_B = 1)$ and main chain's rigidity $\xi = 1$. We focus on the effects of local coupling $\mu_f N$ (stiff hinges with large positive value of $\mu_f N$), the competitions between $\mu_f N$ and LC orientational parameters $\mu_{AA}N$ and $\mu_{BB}N$ and the competition between $\mu_f N$ and the global coupling $\mu_{AB}N$ on the phase behaviors of MCSCLCPs. Furthermore, the phase diagram in μN−f_B plane for $\xi = 1$ is also shown in this work.

Phase Behavior Neglecting Global Coupling ($\mu_{AB}N = 0$). We first investigate the influence of local coupling $\mu_f N > 0$ on the phase behaviors of MCSCLCPs under $\mu_{AB}N = 0$ and $\mu_{AA}N = 0$. Figure 6 shows the order parameters as a function of $\mu_{BB}N$ with $\mu_f N = 0.05$ μN and $f_B = 0.476$. From Figure 6, the side groups B are weakly ordered in the z-direction ($|\lambda_{z,B}| \leq 0.2$) in the region $150 < \mu_{BB}N \leq 170$, forcing the backbone chain A into the xy plane with $\lambda_{z,A} < 0$. When $\mu_{BB}N$ is further increased, the ordering degree of B greatly increases, and A presents oblate shape with the same primary axis as well as B, forming the

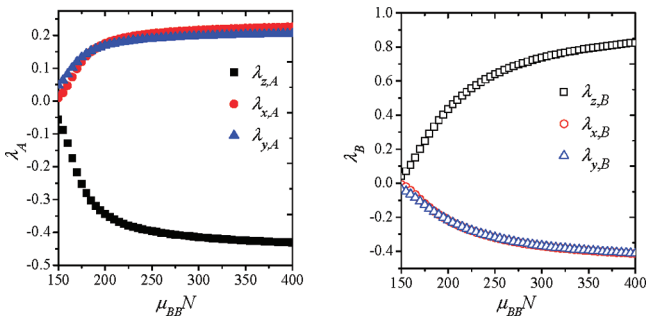

Figure 6. Orientational order parameters λ for MCSCLCPs with $f_B = 0.476$ $(N_A/N_B = 1)$ and $\xi = 1$ as a function of orientational interaction $\mu_{BB}N = \mu N$ in the case of $\mu_f N = 0.05\mu N$, $\mu_{AB}N = 0$, and $\mu_{AA}N = 0$.

dx.doi.org/10.1021/ma2027879 | Macromolecules 2012, 45, 3590−3603

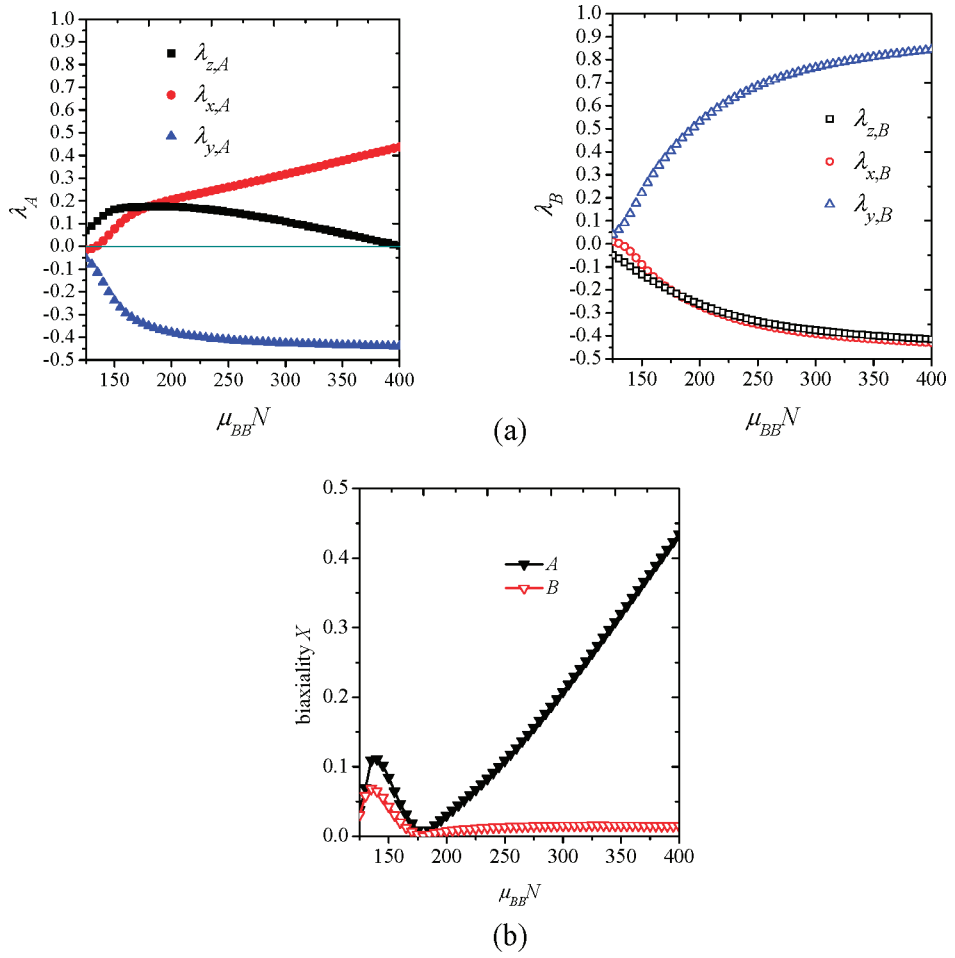

Figure 7. (a) Orientational order parameters λ and (b) the biaxiality parameter X for MCSCLCPs with $f_B = 0.476$ ($N_A/N_B = 1$) and $\xi = 1$ as a function of orientational interaction $\mu_{BB}N = \mu N$ in the case of $\mu_f N = 0.5\mu N$, $\mu_{AB}N = 0$, and $\mu_{AA}N = 0$.

uniaxial phase $N_{PI}(O_AP_B)$. Ignoring all of the global effect on A implies that the backbone is relatively flexible. The local rigidity arising from the linked segments forces the oblate comformation of A, which is similar to the freely joined chain model adopted in ref 29.

However, when $\mu_f N$ is further increased, the backbone with intrinsic bending energy induces different phase behaviors from the completely flexible backbone. Figure 7 shows the stronger local coupling effect with $\mu_f N = 0.5\mu N$, in contrast to Figure 6. Although side groups B order first when the anisotropic phase occurs with increasing their orientational parameter $\mu_{BB}N$, the main chain with some stiffeness ($\xi = 1$) orients along the z-direction induced by the rigid hinge effects. Thus, a weakly ordered uniaxial nematic phase $N_{PII}(P_AO_B)$ is formed at $\mu_{BB}N = 125$. With the further increase of $\mu_{BB}N$, the side groups with high ordering degree display prolate shape with the primary axis along the y-direction. The perpendicular alignment effect of the linkage is also increased by the higher ordered side groups and forces the backbone parallel into the xz plane at $\mu_{BB}N = 180$, forming the $N_{PI}(O_AP_B)$ phase. In the transition region ($130 < \mu_{BB}N < 165$), biaxial phases with small values of biaxiality parameter X occur, shown in Figure 7b. For the first-order unaixial−biaxial phase transitons, we can easily recognize the biaxial phases as long as the biaxiality parameter does not vanish. However, for the second-order phase transitons in this work, the appearance of biaxiality is continuous with the increase of $\mu_{BB}N$. Therefore, for the second-order unaixial−biaxial phase transitons, we define the transition points from uniaxial to biaxial phases as long as one of the biaxiality parameters of the two components is larger than an arbitrary relatively small value, such as 0.05. When $\mu_{BB}N > 210$, the side groups always orient along the y-direction whereas the backbone begins to stretch along the x-axis from the oblate shape in xz plane. Because of the order changes of A, the biaxial phase of the system occurs, forming the $N_{BI}(B_AP_B)$ phase. The biaxial phases are induced by the perpendicular toplogical structures between the main chain and side groups ($\mu_f N$) and main-chain bending feature ξ. It should be noticed that the bending energy ξ incorporated in the wormlike chain model is an essential parameter to form some special biaxial phases. When $\mu_f N$ is strong enough, the local coupling $\exp[-\mu_f N(\mathbf{u}\cdot\mathbf{v})^2]$ first effects on the propagator $q(\mathbf{u},s)$ in eq 21 of the connecting segement, inducing the perpendicular alignment between the side group and its own backbone segment. Then the operater $\nabla_{\mathbf{u}}^2/\xi$ with large value of ξ acting on the $q(\mathbf{u},s)$ in eq 20 drives the adjacent backbone segments to adopt wormlike chain conformation. Therefore, when the values of $\mu_f N$ and ξ are large enough, the biaxial behavior of the backbone N_{BI} can also be obtained even in the absence of the nematic interaction between the main-chain segments, such as $\mu_{AA} = 0$. It is also confirmed in experiments that the flexible backbone also appears as the wormlike chain conformation when the rods are stiffly linked to it.[18] In contrast, if the nematic interaction μ_{AA} is included in the freely jointed chain model without bending energy, we can

dx.doi.org/10.1021/ma2027879 | Macromolecules 2012, 45, 3590−3603

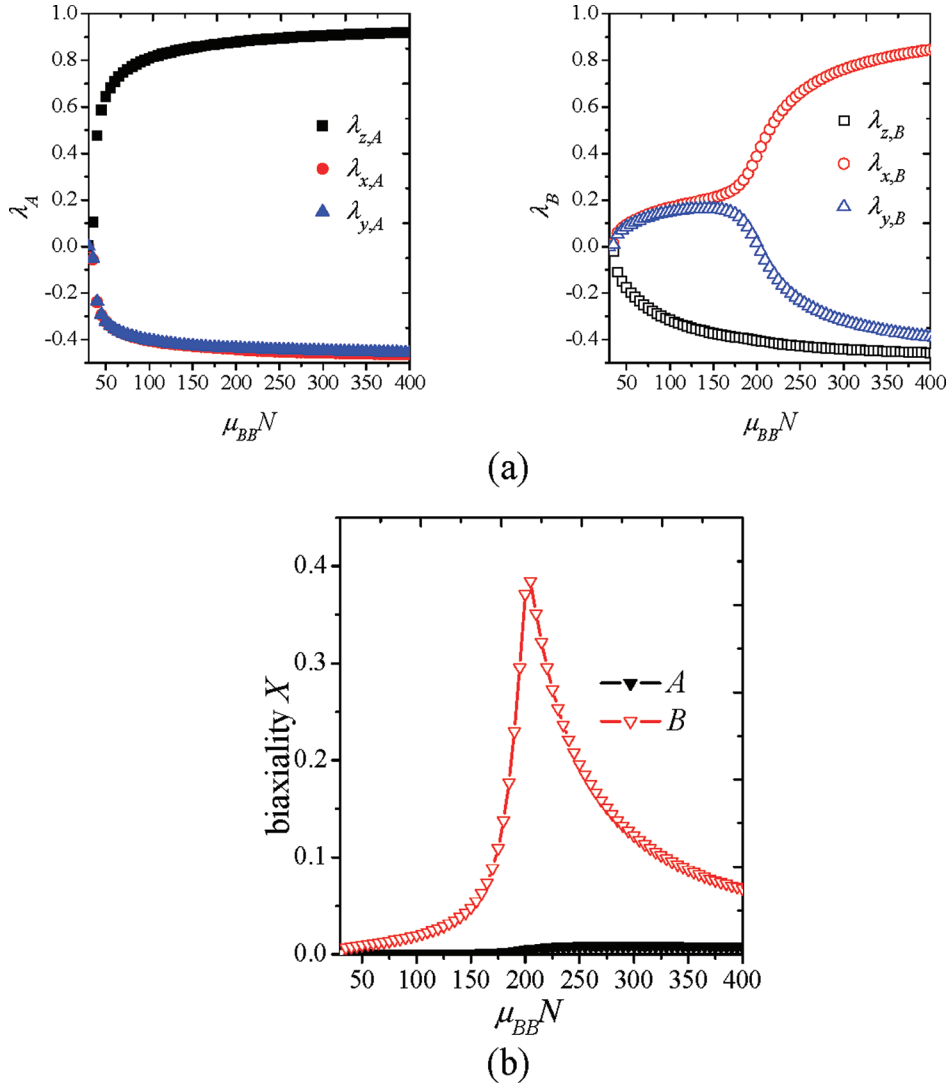

Figure 8. (a) Orientational order parameters λ and (b) the biaxiality parameter X for MCSCLCPs with $f_B = 0.476$ ($N_A/N_B = 1$) and $\xi = 1.0$ as a function of orientational interaction $\mu_{BB}N$ in the case of $\mu_fN = 0.05\mu N$, $\mu_{AA}N = \mu_{BB}N = \mu N$, and $\mu_{AB}N = 0$.

obtain the uniaxial nematic conformation of the main chain just like rod molecules and also the biaxial phase N_{BIII} with the backbone and side groups orientating along their individuals but with orthogonal primary directions. However, the freely jointed chain model cannot describe the biaxial behavior of the backbone such as N_{BI} and side groups such as N_{BII} phases in the following discussion.

The main chain A is treated as a wormlike chain in our model; thus, the orientational interaction of A, $\mu_{AA}N$, should be considered. In contrast to the results of Figure 6, the situations with $\mu_{AA}N = \mu_{BB}N = \mu N$ are shown in Figure 8. With the relatively stiff property ($\xi = 1$), the main-chain ordering influence is quite strong; thus, A orders first at $\mu N = 40$ to form a prolate shape with the primary axis orientated along the z-direction and forces the side groups B into the xy plane, forming the $N_{PII}(P_AO_B)$ phase. Even when $\mu_{BB}N$ is increased from 40 to 400, the A component always orients along the z-direction. Whereas, the components B undergo the transition from the oblate shape oriented in the xy plane to the biaxial nematic structure ordered in the x-direction at $\mu_{BB}N > 150$, forming the biaxial phase of the system $N_{BII}(P_AB_B)$. The order parameters of A are always larger than those of B; thus, the primary order of the system is consistent with the primary order of A, which is coincident with the theoretical results.[31] Moreover, we confirm that the biaxial nematic phase favors more conformation entropy of the system than the parallel orientations of them. The phase transition form N_{PII} to N_{BII} is induced by the competition between the orientational behaviors of LC moiety favoring parallel alignment of two components and the stiff hinge favoring orthogonal alignment.

Phase Behaviors in the Presence of Global Coupling ($\mu_{AB}N \neq 0$). In Figure 9, we focus on the effect of global coupling $\mu_{AB}N$ on the phase behaviors of MCSCLCPs while ignoring the interactions of A segments ($\mu_{AA}N = 0$). In this case, the two effects of $\mu_{AB}N$ favoring parallel alignment of A and B and the perpendicular hinge μ_fN counterbalance each other; thus, the anisotropic phase occurs until $\mu_{AB}N$ controls over μ_fN at large value of $\mu_{BB}N$ ($\mu_{BB}N = 200$). The backbone chain tends to be oblate to gain more chain conformation in the case of $\mu_{AA}N = 0$, and $\mu_{AB}N$ prefers parallel orientations between A and B. Thus, a new uniaxial phase N_O occurs in which both A and B display oblate shapes and the averaged orientational parameters are parallel to each other. The oblate spheroids determined by SANS were also mentioned in experiments.[11]

dx.doi.org/10.1021/ma2027879 | *Macromolecules* 2012, 45, 3590−3603

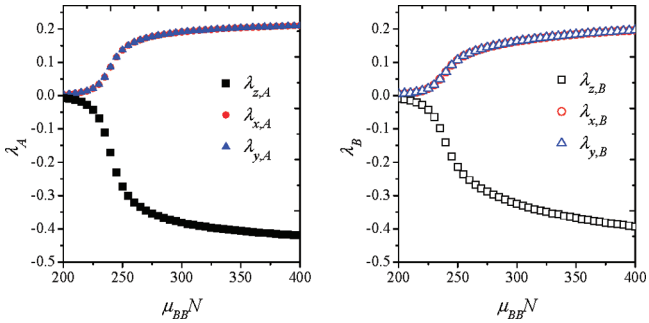

Figure 9. Orientational order parameters λ for MCSCLCPs with f_B = 0.476 (N_A/N_B = 1) and ξ = 1 as a function of orientational interaction $\mu_{BB}N$ in the case of $\mu_fN = 0.05\mu N$, $\mu_{AB}N = \mu_{BB}N = \mu N$, and $\mu_{AA}N = 0$.

If all the orientational parameters are taken into account, i.e., $\mu_{AA}N = \mu_{BB}N = \mu_{AB}N = \mu N$, the phase transitions are more complex. Figure 10 shows the order parameters and biaxiality parameter as a function of μN with local coupling $\mu_fN = 0.05\mu N$. Similar to the phenomenon in Figure 8, the N_{PII} phase occurs at μN = 50 because the main chain *A* orders first along the *z*-direction to form a prolate shape forcing the side groups *B* into the *xy* plane. When μN is further increased, *B* components with comparable volume fraction take the opportunity to order in the *xy* plane and orient along the *x*-direction to gain the beneficial orientational energy at $\mu N \approx 225$, forming the prolate shape of themselves. In the transition region of 175 < μN < 225, the side groups are oriented differently in 3D space, appearing biaxial orientations of *B*. The evolution of the side groups' orientations have an important effect on the main chain *A*, inducing the order parameters of *A* have deviations away from the *z*-axis. From Figure 10b, we see that the maximum value of the biaxiality *X* of *B* occurs at μN = 195, and that of the overall system subsequently occurs at μN = 210. Therefore, the biaxial phase of the system results from the transition from oblate shape to biaxial structure of *B* and the primary order of *A*, resulting in the phase of $N_{BII}(P_AB_B)$. When μN is further increased, the cost of the stretching energy of *A* will be intense due to the ordering of *B*, therefore forming biaxial shapes for both *A* and *B* at $\mu N \approx 275$. However, the separated orientations of *A* along the *z*- and *x*- directions while those of *B* are complementary, reducing the biaxiality of the overall system. We include this phase into N_{BII} phase. After that, the global interactions preferring parallel orientations of the two components compete the perpendicular effect of local coupling, and the conformation entropy of *A* dominates the phase behavoir. In this case, the uniaxial nematic phase N_O is found, similar to Figure 9.

Phase Diagram in μN–f_B Plane for ξ = 1. We present the phase diagram in the μN–f_B plane ($\mu_{AA}N = \mu_{BB}N = \mu_{AB}N = \mu N$) while fixing ξ = 1 and $\mu_fN = 0.5\ \mu N$ in Figure 11. It displays the principal ordered phases N_{PI}, N_{PII}, N_O, N_{BI}, N_{BII}, and N_{BIII} as well as the isotropic phase **I**. In order to compare the relative stability of the phases between isotropic and nematic phase, we started the free enery calculation with both random initial conditions and the given aligned states including uniaxial and biaxial initial fields. For each certain fixed composition, the phase boundary is constructed by comparing the free

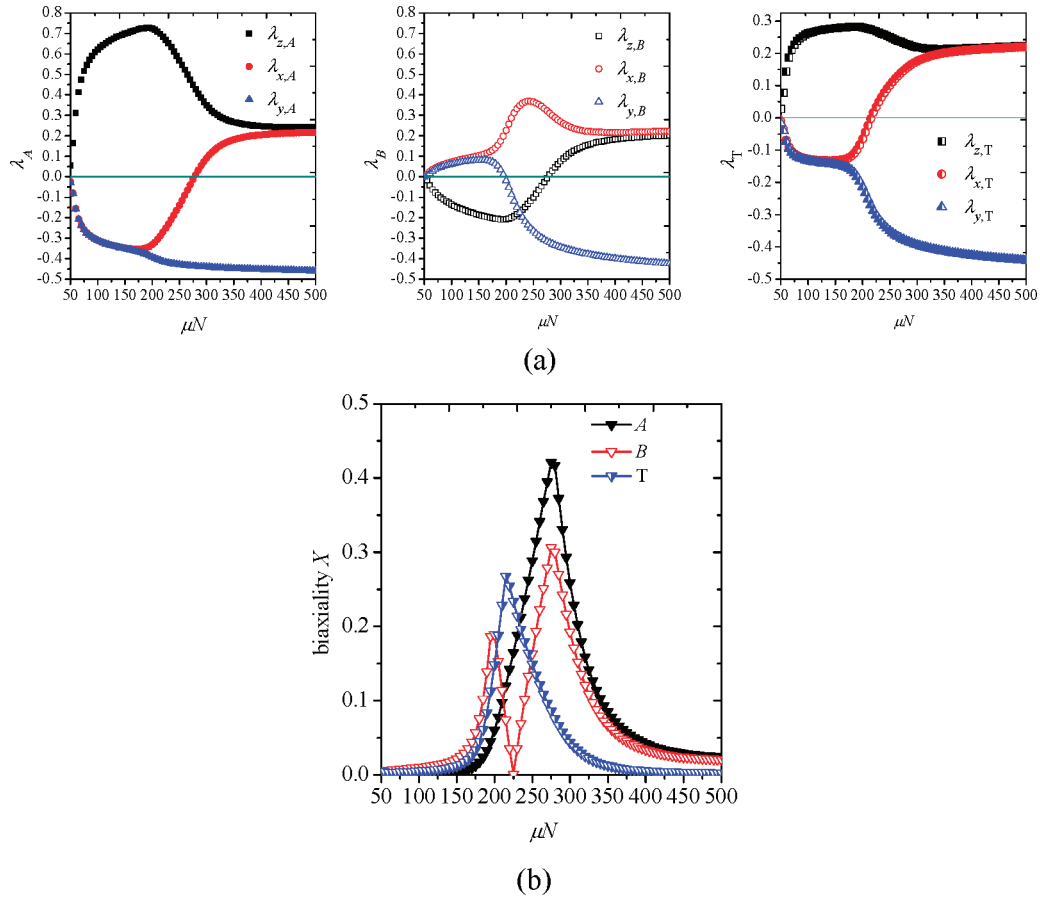

Figure 10. (a) Orientational order parameters λ and (b) the biaxiality parameter *X* for MCSCLCPs with f_B = 0.476 (N_A/N_B = 1) and ξ = 1 as a function of orientational interaction μN in the case of $\mu_fN = 0.05\mu N$ and $\mu_{AA}N = \mu_{BB}N = \mu_{AB}N = \mu N$.

dx.doi.org/10.1021/ma2027879 | *Macromolecules* 2012, 45, 3590–3603

energy of various phases including isotropic phase with the increase of μN by a step of $\Delta\mu N = 5$. The intersection point of these curves of the free energy is decided as the phase boundary point. The symbols in Figure 11 represent the calculated transition points, and the transition lines separating two different phases are simply a guide for the eyes. For each f_B, the discontinuities of the first-order partial derivative of the free energy determine the first-order phase transitions as a function of μN, denoted by the solid lines, otherwise defined as the second-order phase transitions, indicated by the dashed lines. The N'_{BII} (N'_{BI}) phase is biaxial phase where the side groups B (main chain A) display obvious biaxiality, i.e., $X_B \geq 0.05$ ($X_A \geq 0.05$), whereas the overall system displays prolate ellipsoid shape ($X_T < 0.05$) with such a small value volume fraction of the biaxial component. We distinguish them from N_{BII} and N_{BI} phases by dotted curves, respectively. In this phase diagram, the N_{PIII} phase in Figure 1 is not found, which is different from some theoretical reports about SCLCPs and MCSCLCPs.[27,31] It is reasonable that the effect of each side group and its local coupling have entered in the modified diffusion equation of the backbone and can accurately describe the topological structures of MCSCLCPs. Therefore, the backbone and the side groups prefer to be perpendicular between each other as long as one of the component dominates the order of system as increasing of μN.

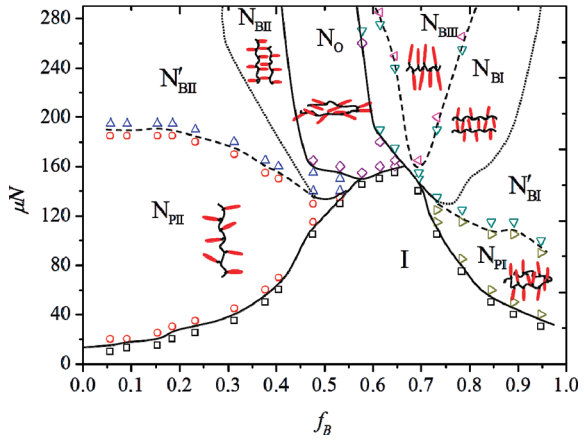

Figure 11. Phase diagram plotted in the μN–f_B plane for MCSCLCPs with the stiff hinge ($\mu_f N = 0.5\mu N$) in the case of the main-chain flexibility $\xi = 1.0$ and $\mu_{AA}N = \mu_{BB}N = \mu_{AB}N = \mu N$. The symbols represent the calculated transition points, and the transition lines are simply a guide for the eyes between the two side phases. The solid lines denote the first-order phase transitions, and the dashed lines denote second-order phase transitions. The $N'_{BII}(N'_{BI})$ phase separated from $N_{BII}(N_{BI})$ phase by dotted curves are biaxial phases where the side groups B (main chain A) display obvious biaxiality, i.e., $X_B \geq 0.05$ ($X_A \geq 0.05$), whereas the overall system displays prolate ellipsoid shape ($X_T < 0.05$).

To the left of the phase diagram, similar to the above analysis, the effect of the backbone with large volume fraction is dominant, and the side groups are forced into the xy plane, forming N_{PII} phase. With increasing of μN, the N'_{BII} phase is separated from N_{PII} phase, which is actually an prolate ellipsoid of the system, whereas the side groups B with small volume fraction display obvious biaxiality ($X_B \geq 0.05$). When μN is further increasd, the biaxial phase N_{BII} occurs because of the ordering of B. Moving toward to the middle of the phase diagram, the interaction effects of the A and B are comparable,

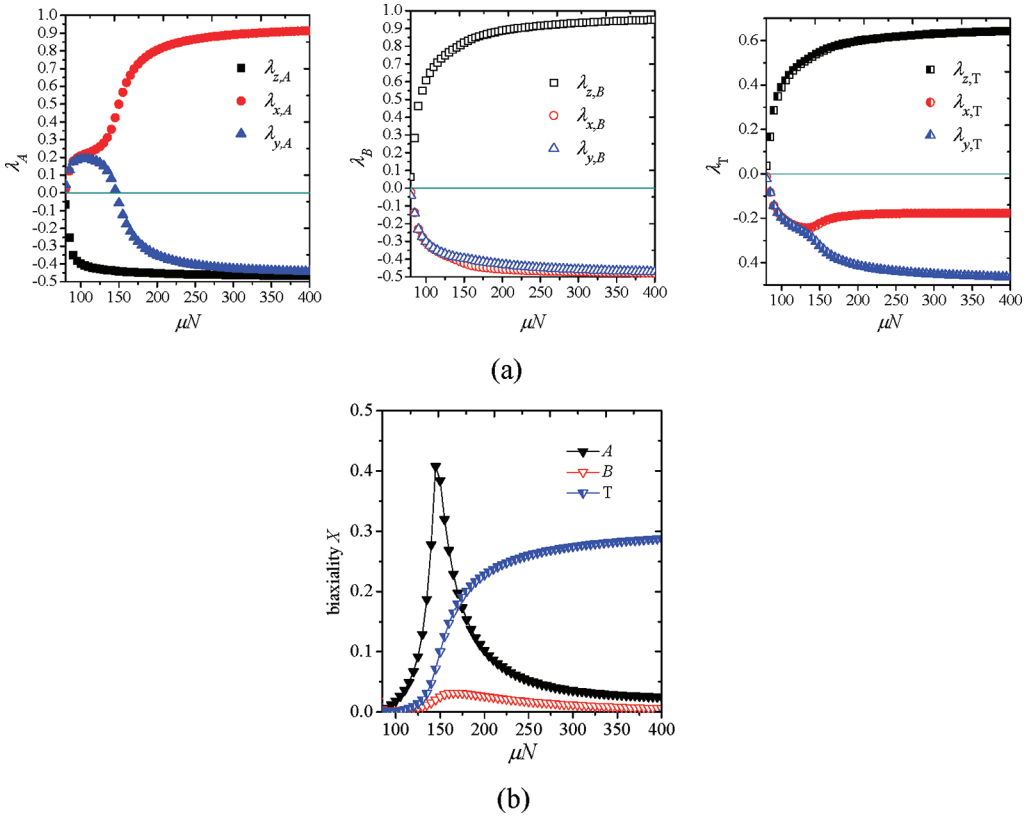

Figure 12. (a) Orientational order parameters λ and (b) biaxiality parameter X for MCSCLCPs with $f_B = 0.784$ ($N_A/N_B = 1/4$) and $\xi = 1$ as a function of orientational interaction μN in the case of $\mu_f N = 0.5\mu N$ and $\mu_{AA}N = \mu_{BB}N = \mu_{AB}N = \mu N$.

dx.doi.org/10.1021/ma2027879 | Macromolecules 2012, 45, 3590–3603

increasing the complexity of the phase transition. The uniaxial nematic phase N_O is formed when the global interactions dominate over the local coupling with large value of μN. Furthermore, due to the competitions between the parallel nematic interactions and the perpendicular local hinge effect, larger value of μN (lower temperature) are required to produce the phase transition from isotropic to anisotropic phase than the situation without local coupling effect ($\mu_f N = 0$) in Figure 4a, especially for almost equal volume fraction of the two components. It is also reported in the experiment that the introduction of stiff phenylsulfonyl side groups decreased the clearing temperature of the pure semiflexible polymers.[56]

To the right of the phase diagram, the orientational effect of the side groups become stronger. Increasing μN from the isotropic phase results in N_{PI}, N_{BI}, and N_{BIII} in turn. For instance, we analyze that phase transitions with $f_B = 0.784$ in detail, shown in Figure 12. The side groups begin to order at $\mu N = 80$ and force the backbone into the xy plane, forming the N_{PI} phase. The prolate shapes of B are always stable during the simulation region of μN. However, with the increase of μN, the backbone orders in the x-direction and displays biaxiality at $\mu N = 115$ with $X_A > 0.05$, as shown in Figure 12b. The biaxiality of the overall system occurs at $\mu N = 145$ with $X_T > 0.05$ following the biaxiality of A. When μN is further increased, the backbone stretches with strong ordering degree in the x-direction, and the biaxiality disappears at $\mu N > 270$ with $X_A < 0.05$. In this case, A and B present prolate shape of themselves, whereas the primary axises of A and B are perpendicular to each other, inducing the biaxial phase of the overall system with the order parameters parallel to xz plane, i.e., $N_{BIII}(P_AP_B)$. The biaxial phase N_{BIII} has never been reported before. In our study, the N_{BIII} phase is typically found at $0.65 < f_B < 0.7$, where the biaxiality of the overall system X_T is rapidly increased to 0.3 with $X_A < 0.05$ and $X_B < 0.02$ upon the appearance of the anisotropic phase. The biaxial phase N_{BIII} is obtained in the case of high backbone stiffness, comparable μ_{AA} and μ_{BB}, and stiff hinges, consistent with the biaxial molecular orientation in the experiments about the combined main-chain and side groups LC polymers.[10,16] Furthermore, the biaxial nematic phases are fond of side-on SCLCPs in experiments.[22,57] This is our bold guess, and a further study with both order parameters and microscopic densities distribution is expected to clarify the rich phase behaviors of side-on SCLCPs.

CONCLUSIONS

We use the SCFT method to investigate the isotropic−anisotropic phase transitions of the MCSCLCPs and the conformation of the system. A universal model is developed by treating the backbone as a wormlike chain with varying rigidity degree and attached with the rigid side groups hinged to it. The global nematic coupling and the local hinge effects are adopted to describe the interactions between the backbone and the side groups. The global nematic interactions favoring the parallel alignment between backbone segments, between the backbone side groups, and between the side mesogens are all described by Maier−Saupe orientational interactions. Whereas the local coupling effect involves the instantaneous values depending on the orientation vectors of the backbone segment and its own LC side groups, which was first proposed by Wang and Wang[29] for investigating the chain conformation of SCLCPs. Furthermore, the local coupling effect and the probability of each side group all act on the modified diffusion equation of the wormlike main chain, which is implemented by the pseudospectral operator splitting algorithm to obtain the chain propagator $q(\mathbf{u},s)$. The orientation degrees of the backbone chain and the side groups are all described by the corresponding unit vectors $\mathbf{u}\{\theta,\varphi\}$. By numerically solving the SCFT equations, we investigate the effects of rigidity of the main chain ξ, the self-nematic interactions $\mu_{AA}N$ and $\mu_{BB}N$, the global coupling $\mu_{AB}N$, the strength of local hinge $\mu_f N$, and the volume fraction f_B on the liquid crystal behaviors of MCSCLCPs. Rich ordered phases including uniaxial phases N_{PI}, N_{PII}, N_{PIII}, and N_O and biaxial phases N_{BI}, N_{BII}, and N_{BIII} are obtained in this work.

When the hinge is flexible, i.e., $\mu_f N = 0$, only prolate uniaxial nematic phase N_{PIII} are obtained where both of the main chain and side groups are parallelly ordered between each other. In this case, the relativley stiff main chain with intrinsic bending modulus dominates the phase transition from isotropic phase to nematic phases. Whereas for the relatively flexible backbone, the effects of side groups play more important role in the right of the phase diagram because the strength of side-chain interaction is governed by their volume fraction.

When the hinges are stiff with a large positive value of $\mu_f N$, the side groups prefer to be linked perpendicularly to the backbone and the comb geometrical structure of MCSCLCPs dominates the phase behaviors. The competitions between the global Maier−Saupe interaction preferring parallel orientations of the system, the perpendicular tendency of the two components, and the stretching energy of main chain with some bending modulus ξ but having to satisfy the conformation of maximum entropies result in complex transitions between uniaxial phases and biaxial phases. The uniaxial phases N_{PI} and N_{PII} are dominated by the order of the side groups and the main chain, respectively. The backbone of N_{PI} and side groups of N_{PII} forms oblate shapes. With the increase of μN, the biaxial phases N_{BI} and N_{BII} occur because the backbone chain and the side groups tend to order along their primary axis, respectively. The biaxial orderings of the backbone in N_{BI} and side groups in N_{BII} phases result from the accurate numerical calculation of the wormlike chain model with bending energy ξ. The new uniaxial phase N_O occurs when the global coupling effects with comparable volume fractions of backbone and side groups defeat the local coupling effects as well as the maximal entropy of the main chain. When the backbone has high chain stiffness and μ_{AA} is comparable to μ_{BB}, another new phase N_{BIII} is found as a biaxial phase, whereas the backbone and side groups are orientated along their individuals but with orthogonal primary directions. Furthermore, in contrast to the situation without local coupling effect, the phase transition from isotropic to anisotropic phase requires larger value of μN (lower temperature).

AUTHOR INFORMATION

Corresponding Author

*E-mail: pingtang@fudan.edu.cn.

Notes

The authors declare no competing financial interest.

ACKNOWLEDGMENTS

We thank financial support from the National Basic Research Program of China (Grant 2011CB605700). Funds from the NSF of China (Grants 20990231 and 91127033) are also acknowledged.

REFERENCES

(1) Ikeda, T.; Tsutsumi, O. *Science* **1995**, *268*, 1873.
(2) Blackwood, K. M. *Science* **1996**, *273*, 909.
(3) Ahn, S. K.; Deshmukh, P.; Gopinadhan, M.; Osuji, C. O.; Kasi, R. M. *ACS Nano* **2011**, *5*, 3085.
(4) Chakrabarti, P.; Pal, D. *Prog. Biophys. Mol. Biol.* **2001**, *76*, 1.
(5) de Gennes, P. G.; Prost, J. *The Physics of Liquid Crystals*, 2nd ed.; Clarendon Press: Oxford, UK, 1993.
(6) Wessels, P. P. F.; Mulder, B. M. *J. Phys.: Condens. Matter* **2006**, *18*, 9359.
(7) Reck, B.; Ringsdorf, H. *Makromol. Chem., Rapid Commun.* **1985**, *6*, 291.
(8) McArdle, C. B. *Side Chain Liquid Crystal Polymers*; Blackie: Glasgow, 1989.
(9) Zhou, Q. F.; Zhu, X. L.; Wen, Z. Q. *Macromolecules* **1989**, *22*, 491.
(10) Xie, H. L.; Jie, C. K.; Yu, Z. Q.; Liu, X. B.; Zhang, H. L.; Shen, Z. H.; Chen, E. Q.; Zhou, Q. F. *J. Am. Chem. Soc.* **2010**, *132*, 8071.
(11) Kempe, M. D.; Kornfield, J. A.; Lal, J. *Macromolecules* **2004**, *37*, 8730.
(12) Lecommandoux, S.; Noirez, L.; Achard, M. F.; Hardouin, F. *J. Phys. II* **1996**, *6*, 1231.
(13) Craig, A. A.; Imrie, C. T. *Macromolecules* **1999**, *32*, 6215.
(14) Riala, P.; Andreopoulou, A.; Kallitsis, J.; Gitsas, A.; Floudas, G. *Polymer* **2006**, *47*, 7241.
(15) Craig, A. A.; Imrie, C. T. *Macromolecules* **1995**, *28*, 3617.
(16) Piao, X. L.; Kim, J. S.; Yun, Y. K.; Jin, J. I.; Hong, S. K. *Macromolecules* **1997**, *30*, 2294.
(17) Percec, V.; Keller, A. *Macromolecules* **1990**, *23*, 4347.
(18) Kikuchi, M.; Lien, L. T. N.; Narumi, A.; Jinbo, Y.; Izumi, Y.; Nagai, K.; Kawaguchi, S. *Macromolecules* **2008**, *41*, 6564.
(19) Rousseau, D.; Marty, J. D.; Mauzac, M.; Martinoty, P.; Brandt, A.; Guenet, J. M. *Polymer* **2003**, *44*, 2049.
(20) Cotton, J. P.; Hardouin, F. *Prog. Polym. Sci.* **1997**, *22*, 795.
(21) Lecommandoux, S.; Achard, M. F.; Hardouin, F.; Brulet, A.; Cotton, J. P. *Liq. Cryst.* **1997**, *22*, 549.
(22) Severing, K.; Saalwachter, K. *Phys. Rev. Lett.* **2004**, *92*, 125501.
(23) Finkelmann, H.; Rehage, G. *Adv. Polym. Sci.* **1984**, *60−1*, 97.
(24) Vasilenko, S. V.; Shibaev, V. P.; Khokhlov, A. R. *Macromol. Chem. Phys.* **1985**, *186*, 1951.
(25) Auriemma, F.; Corradini, P.; Vacatello, M. *J. Chem. Phys.* **1990**, *93*, 8314.
(26) Brochard, F.; Jouffroy, J.; Levinson, P. *J. Phys. (Paris)* **1984**, *45*, 1125.
(27) Wang, X. J.; Warner, M. *J. Phys. A: Math. Gen.* **1987**, *20*, 713.
(28) Renz, W.; Warner, M. *Proc. R. Soc. London, Ser. A* **1988**, *417*, 213.
(29) Wang, R.; Wang, Z. G. *Macromolecules* **2010**, *43*, 10096.
(30) Carri, G. A.; Muthukumar, M. *J. Chem. Phys.* **1998**, *109*, 11117.
(31) Bladon, P.; Warner, M.; Liu, H. *Macromolecules* **1992**, *25*, 4329.
(32) Renz, W. *Mol. Cryst. Liq. Cryst.* **1988**, *155*, 549.
(33) Kratky, O.; Porod, G. *Recl. Trav. Chim* **1949**, *68*, 1106.
(34) Drolet, F.; Fredrickson, G. H. *Phys. Rev. Lett.* **1999**, *83*, 4317.
(35) Wang, R.; Jiang, Z. B.; Hu, J. L. *Polymer* **2005**, *46*, 6201.
(36) Vroege, G. J.; Odijk, T. *Macromolecules* **1988**, *21*, 2848.
(37) Cui, S. M.; Akcakir, O.; Chen, Z. Y. *Phys. Rev. E* **1995**, *51*, 4548.
(38) Duchs, D.; Sullivan, D. E. *J. Phys.: Condens. Matter* **2002**, *14*, 12189.
(39) Song, W. D.; Tang, P.; Zhang, H. D.; Yang, Y. L.; Shi, A. C. *Macromolecules* **2009**, *42*, 6300.
(40) Gao, J.; Tang, P.; Song, W. D.; Yang, Y. L. *Soft Matter* **2011**, *7*, 5208.
(41) Song, W. D.; Tang, P.; Qiu, F.; Yang, Y. L.; Shi, A. C. *Soft Matter* **2011**, *7*, 929.
(42) Fredrickson, G. H. *The Equilibrium Theory of Inhomogenous Polymers*; Clarendon Press: Oxford, 2005.
(43) Chantawansri, T. L.; Bosse, A. W.; Hexemer, A.; Ceniceros, H. D.; Garcia-Cervera, C. J.; Kramer, E. J.; Fredrickson, G. H. *Phys. Rev. E* **2007**, *75*, 031802.
(44) Adams, J. C.; Swarztrauber, P. N. SPHEREPACK 3.1: A Model Development Facility, 2003.
(45) Pryamitsyn, V.; Ganesan, V. *J. Chem. Phys.* **2004**, *120*, 5824.
(46) Yang, G. A.; Tang, P.; Yang, Y. L.; Wang, Q. A. *J. Phys. Chem. B* **2010**, *114*, 14897.
(47) Shah, M.; Pryarnitsyn, V.; Ganesan, V. *Macromolecules* **2008**, *41*, 218.
(48) Jiang, Y.; Zhang, W. Y.; Chen, J. Z. Y. *Phys. Rev. E* **2011**, *84*, 041803.
(49) Davidson, P.; Noirez, L.; Cotton, J. P.; Keller, P. *Liq. Cryst.* **1991**, *10*, 111.
(50) Hessel, F.; Finkelmann, H. *Polym. Bull.* **1985**, *14*, 375.
(51) Fredrickson, G. H.; Ganesan, V.; Drolet, F. *Macromolecules* **2002**, *35*, 16.
(52) Chen, Z. Y. *Macromolecules* **1993**, *26*, 3419.
(53) Chandrasekhar, S.; Sadashiva, B. K.; Ratna, B. R.; Raja, V. N. *Pramana* **1988**, *30*, L491.
(54) Matsuyama, A. *Mol. Cryst. Liq. Cryst.* **2011**, *540*, 42.
(55) Chen, X. F.; Shen, Z. H.; Wan, X. H.; Fan, X. H.; Chen, E. Q.; Ma, Y. G.; Zhou, Q. F. *Chem. Soc. Rev.* **2010**, *39*, 3072.
(56) Chang, S.; Han, C. D. *Macromolecules* **1996**, *29*, 2103.
(57) Hessel, F.; Herr, R. P.; Finkelmann, H. *Macromol. Chem. Phys.* **1987**, *188*, 1597.